Simulation

Simulation: Transactions of the Society for Modeling and Simulation International
88(9) 1116–1128

DOI: 10.1177/0037549712441368
sim.sagepub.com
SAGE SCS

Notional all-electric ship systems integration thermal simulation and visualization

JVC Vargas[1], JA Souza[1], R Hovsapian[1], JC Ordonez[1], T Chiocchio[1], J Chalfant[2], C Chryssostomidis[2] and E Dilay[1]

Abstract

This work presents a simplified mathematical model for fast visualization and thermal simulation of complex and integrated energy systems that is capable of providing quick responses during system design. The tool allows for the determination of the resulting whole system temperature and relative humidity distribution. For that, the simplified physical model combines principles of classical thermodynamics and heat transfer, resulting in a system of three-dimensional (3D) differential equations that are discretized in space using a 3D cell-centered finite volume scheme. As an example of a complex and integrated system analysis, 3D simulations are performed in order to determine the temperature and relative humidity distributions inside an all-electric ship for a baseline medium voltage direct current power system architecture, under different operating conditions. A relatively coarse mesh was used (9410 volume elements) to obtain converged results for a large computational domain (185m $\times$ 24m $\times$ 34m) containing diverse equipment. The largest computational time required for obtaining results was 560 s, that is, less than 10 min. Therefore, after experimental validation for a particular system, it is reasonable to state that the model could be used as an efficient tool for complex and integrated systems thermal design, control and optimization.

Keywords

medium voltage direct current architecture, temperature field, relative humidity field, thermal management, early-stage design tool

1. Nomenclature

A	volume element (VE) face area, m^2
c	specific heat, J kg^{-1} K^{-1}
C	heat capacity rate, W K^{-1}
g	gravity, m s^{-2}
h	heat transfer coefficient, W m^{-2} K^{-1}
H	swept height, m
I	local average sun irradiation, W m^{-2}
k	thermal conductivity, W m^{-1} K^{-1}
k_w	wall thermal conductivity, W m^{-1} K^{-1}
l	VE side (length, width or height), m
L	swept length, m
$\dot{m}$	mass flow rate, kg s^{-1}
n_{eq}	total number of internal fluid cooled equipment in a zone
N	total number of VEs
NTU	number of heat transfer units
p_v	vapor pressure, N m^{-2}
p_{vs}	water saturation pressure, N m^{-2}
Pr	Prandtl number
$\dot{Q}$	heat transfer rate, W
R	thermal resistance, m^{-2} K W^{-1}
Ra	Rayleigh number
Re	Reynolds number
t	time, s
t_w	wall thickness, m
T	temperature, K
U	global heat transfer coefficient, W m^{-2} K^{-1}
v	velocity, m s^{-1}
V	volume, m
x, y, z	Cartesian coordinates, m

[1]Department of Mechanical Engineering and Center for Advanced Power Systems, Florida State University, Tallahassee, USA
[2]MIT Sea Grant Design Laboratory, Massachusetts Institute of Technology, Cambridge, USA

Corresponding author:
JVC Vargas, Department of Mechanical Engineering and Center for Advanced Power Systems, Florida State University, Tallahassee, FL 32310, USA.
Email: jvargas@caps.fsu.edu

1.1 Greek letters

α	absorptivity
α_T	thermal diffusivity, $m^2\ s^{-1}$
β	coefficient of volumetric thermal expansion, K^{-1}
ε	emissivity
ε_{hx}	heat exchanger effectiveness, Equation (18)
ε_{mesh}	mesh refinement relative error, Equation (25)
η	thermal efficiency
ν	kinematic viscosity, $m^2\ s^{-1}$
ρ	density, $kg\ m^{-3}$
σ	Stefan–Boltzmann constant, 5.6731028 $W\ m^{-2}\ K^{-4}$
ϕ	relative humidity

1.2 Subscripts

a	adjacent VE number
b	bottom
c	solid VE number
conv	convection
cw	chilled fluid unit
e	east
ext	exterior
f	fluid
fw	internal fluid
film	film
gen	generation in a VE
hx	heat exchanger
i	VE number
in	inlet
int	interior
j	external wall
l	VE face
m	direction
max	maximum
min	minimum
n	north
neigh	neighbor
p	gas at constant pressure
rad	radiation
s	south
sw	external fluid
t	top
w	west
x	*x*-direction
y	*y*-direction
z	*z*-direction
0	initial condition
∞	exterior air
$\lvert \cdot \rvert$	absolute value
$\lVert \cdot \rVert$	Euclidean norm

2. Introduction

The research development of an all-electric ship requires the assessment of the integrated systems' thermal and electrical response in acceptable time. Therefore, a simulation tool that is capable of providing quick responses during early stages of ship design is needed. In this way, thermal viability of the Navy's future all-electric ships could be demonstrated through simulation and modeling at the ship system level. For that, the development of physics-based, electrical-thermal-mechanical models capable of addressing the transient nature of the problem in a global sense is needed. Current methodologies for the thermodynamic optimization of complex systems are experimentally and computationally expensive. An illustrative example is the application of numerical methods to conservation partial differential equations in diverse phenomena, such as in complex integrated energy systems, which leads to high cost and computational time even for the simulation of a few selected cases and thus essentially precludes the possibility of an optimization study.

Liu et al.[1] recently presented an overview of typical methodologies of energy systems engineering, comprising superstructure-based modeling, mixed-integer linear and non-linear programming, multi-objective optimization, optimization under uncertainty, and life-cycle assessment, while contending that all energy-producing alternatives should be taken into consideration in an integrated way in order to cope with current global energy and environmental challenges. The study concluded that methodological modeling and an optimization framework are needed to address complex energy and environmental problems. Recent studies[2,3] state that process integration, which is a key enabler to increasing efficiency in energy-generation industries, leads to increasingly complex dynamic behavior, such that tightly integrated designs continue to be regarded with caution owing to the dynamics and control difficulties that they pose. This complexity demands simple and computationally fast component models that can be combined to produce the global system response.

In the direction of computationally fast and efficient models, the thermal response of complex and integrated systems has been investigated through a simplified physical model in previous studies[4–6] for electronic packages and all-electric ships. Proceeding with the effort, towards the goal of total solutions to thermal and electrical management, a reliable and comprehensive computational visualization tool was also developed.[7,8] In this way, visualization that geographically lays out the integrated system's critical thermal management systems and addresses adaptive control issues in a system context will be possible.

An example of complex and integrated systems is the all-electric ship, which is expected to make more efficient

use of on-board power and to cut fuel use. The technology is also expected to help meet future requirements for high-power weapons, such as the electromagnetic gun, high-power microwave and high-energy lasers. The US Navy's Office of Naval Research (ONR) created five 'focus areas' for the development of the all-electric ship. They are power generation; distribution and control; energy storage; heat transfer and thermal management; and motors and actuators, as reported by Wagner.[9] The five areas are highly interdependent for synchronized and optimal operation. Heat generation is present in all of them, in different levels, from low to high, for example, as a result of electromagnetic launcher operation,[10] propulsion,[11] and all other ship systems. Therefore, poor thermal management could eventually lead to unexpected performance and failure of mechanical-electrical systems to the detriment of the ship's combat mission.[12]

2.1 Objectives

The bibliographic review demonstrated that there is a need for the development of a tool that is capable of complex integrated energy systems design in low computational time. Such a tool is expected to be an important asset for the solution of issues in the areas of energy conversion and conservation, the optimal use of energy resources, analysis and optimization of energy processes, mitigation of environmental pollutants, and sustainable energy systems. Therefore, the main objectives of this paper are as follows.

1. To upgrade the simplified mathematical model introduced previously for electronic packages and all-electric ships[4–6] by including fresh and sea water (or any other cooling fluid) cooled systems throughout the global system, and the assessment of both steady-state and transient behaviors.
2. To develop a computational tool that requires low computational time to provide solutions for each tested configuration in order to allow for an effective design and optimization procedure.
3. To test the model with the computational simulation of a notional all-electric ship for the so-called baseline medium voltage direct current (MVDC) architecture. For that, a three-dimensional (3D) simulation is performed in order to determine the temperature and relative humidity distributions inside the all-electric ship, and representative operating conditions are analyzed.

3. Mathematical model

A 3D cell-centered finite volume scheme was used to discretize the domain and numerically solve the problem.[13] The innovation in the present model is that a coarse mesh is built with lumped control volumes. This is possible through the use of theoretical and empirical heat transfer correlations available in the literature to simplify the modeling equations, and stabilize and speed up the computations. The control volumes consist of bounding boxes that contain a fluid (e.g. air, water), solid equipment, or both.

Since the main objective is to obtain accurate temperature and relative humidity distributions, whenever forced convection is present, the required flow field in the domain is imposed approximately, based on the knowledge of external environmental conditions (e.g. wind and sea water speed) and internal components (e.g. mass flow rates, fans, turbines). Therefore, the governing equations are only the mass and energy conservation principles applied to each VE.

The combination of the proposed simplified physical model with the adopted finite volume scheme for the numerical discretization of the differential equations is called a volume element model (VEM). The model takes into account the existence of element internal heat sinks (or sources) and the heat transfer processes across all element faces, by conduction, convection, and radiation (e.g. sun incidence on the domain boundaries).

The model introduced previously by the authors for electronic packages and all-electric ships[4–6] was validated experimentally for electronic packages by direct comparison with laboratory measurements.[4] Although the model had simplifying assumptions, the experimental validation demonstrated that the model captured the expected system physical trends, so that it could be used for any complex and integrated system design, simulation, control, and optimization purposes. Therefore, in this work the model introduced previously by the authors[4–6] has been improved to include systems cooled by fresh and sea water (or any other cooling fluid) throughout the global system.

Figure 1 shows a typical cell (or VE) that may contain either fluid and/or solid material, according to the element type. Each element interacts with the other adjacent elements, according to the energy equation (first law of thermodynamics) applied to the cell, as follows:

$$\frac{dT_i}{dt} = \frac{1}{(\rho\ V\ c)_i}\left(\sum_{j=e,\,w,\,t,\,b,\,n,\,s} \dot{Q}_j + \dot{Q}_{gen} + \dot{Q}_{conv}\right)_i \quad (1)$$

where $1 \le i \le N$, with N being the total number of elements in the mesh, T_i are the temperatures of each VE, ρ is the density of the material inside the VE (fluid and/or solid), V is the total cell volume, c is either the specific heat of the solid/liquid or the specific heat at constant volume of the gas inside the VE (c_v), $\dot{Q}_e$, $\dot{Q}_w$, $\dot{Q}_t$, $\dot{Q}_b$, $\dot{Q}_n$, $\dot{Q}_s$ and $\dot{Q}_{gen}$ are the heat transfer rates across the east, west, top, bottom, north, and south faces of each VE and the heat sink or source inside the element, respectively, and $\dot{Q}_{conv}$ is the net heat transfer rate collected/rejected through convection by one or more fluid streams (cooling fluids, e.g. fresh or sea water) that flow through the VE.

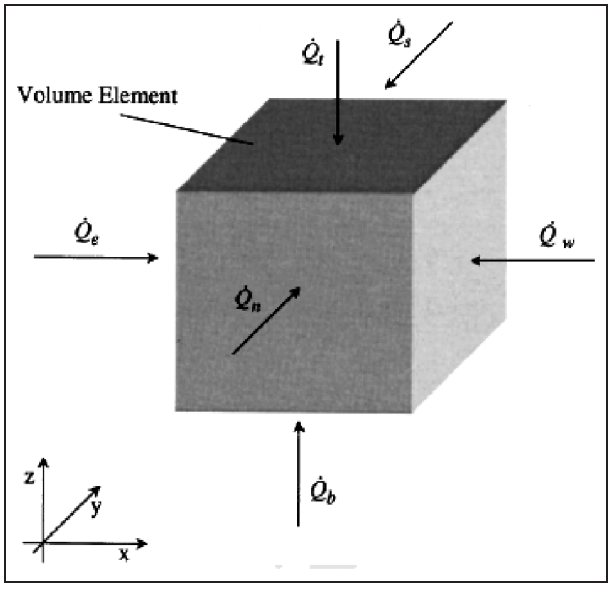

Figure 1. Typical volume element (VE) with heat transfer interactions.

The system of ordinary differential equations defined by Equation (1) formulates the initial value problem to be solved, depicting the temperature field inside the integrated system at any instant of time, for given initial conditions T_{i0}.

Next, the relative humidity at each air element (relative humidity field) follows from the temperature field, by assuming a known initial relative humidity condition, ϕ_{i0}. Firstly, the initial vapor pressure is calculated as follows:

$$p_{v,\,i} = \varphi_{i0} . p_{vs}(T_{i0}) \tag{2}$$

where $p_{v,i}$ is the cell partial vapor pressure, ϕ_{i0} is the cell initial relative humidity, and $p_{vs}(T_{i0})$ is the water saturation pressure at T_{i0}.

It is assumed that the absolute humidity in each VE remains approximately constant during the entire simulation. Hence, the relative humidity at each element that contains air is computed from

$$\varphi_i = \frac{p_{v,\,i}}{p_{vs}(T_i)} \tag{3}$$

where ϕ_i is the relative humidity of the cell and $p_{vs}(T_i)$ is the water saturation pressure at temperature T_i. When the element contains solid equipment (or liquids), a zero value is assigned to it, that is, $\phi_i = 0$.

3.1 Heat transfer rates across the element faces

Empirical correlations[14,15] are utilized to calculate the heat transfer rates across the faces of each VE. In the present formulation, three types of energy interaction are possible: (i) fluid–solid; (ii) fluid–fluid; or (iii) solid–solid. Each element has four side faces that have been named east, west, north, and south, plus a top and a bottom face. There are two possibilities for each face: the face is either in contact with the exterior or with another element.

3.1.1 Element face in contact with the exterior. The element could have solid equipment or fluid in it and one or more faces could be in contact with the exterior. Heat transfer is taken into account by conduction, convection, and radiation as appropriate.

The radiation heat transfer rate across the element face is calculated by

$$\dot{Q}_{rad,\,i,\,j} = A_{i,\,j}\left\{\alpha_j I - \varepsilon_j \sigma\left(T_{i,\,j}^4 - T_{ext}^4\right)\right\}, j = e, w, n, s, t, b \tag{4}$$

where the first term in the curly brackets represents the portion of the average sun irradiation[16] absorbed by the face, when there is sun incidence; $T_{ext} = T_\infty$ (exterior air temperature) or $T_{ext} = T_{sw}$ (other external surrounding fluid temperature, e.g. sea water); α and ε are the element face absorptivity and emissivity, respectively; σ is the Stefan–Boltzmann constant; and $A_{i,j}$ is the element face area. It is also assumed that $I = 0$ at the surfaces in contact with sea water.

The total heat transfer rate (radiation, conduction, and convection) across the face of the element is therefore computed as follows:

$$\dot{Q}_{i,\,j} = \dot{Q}_{rad,\,i,\,j} + U_{i,\,j} A_{i,\,j} (T_{ext} - T_i)\,,\ j = e, w, n, s, t, b \tag{5}$$

where the global heat transfer coefficient, $U_{i,j}$, is given by

$$U_{i,\,j} = \frac{1}{R_{i,\,j}} \tag{6}$$

$$R_{i,\,j} = \frac{l_{i,\,j}/2}{k_i} + \frac{t_w}{k_w} + \frac{1}{h_{ext}} \text{ (solid VE)} \tag{7}$$

or

$$R_{l,\,i} = \frac{1}{h_{\text{int}}} + \frac{t_w}{k_w} + \frac{1}{h_{ext}} \text{ (air VE)} \tag{8}$$

where $l_{i,j}$ is either the cell length or width, k_i is the cell thermal conductivity, t_w and k_w are the wall thickness and thermal conductivity, respectively, and h_{int} and h_{ext} are the interior and exterior convection heat transfer coefficients.

The heat transfer coefficient, h, is calculated for

a) natural convection[14,15]

$$h = \frac{k_f}{H}\left\{0.825 + \frac{0.387\,Ra_H^{1/6}}{\left[1 + (0.492/Pr)^{9/16}\right]^{8/27}}\right\}^2 \tag{9}$$

where k_f is the fluid thermal conductivity, Pr is the Prandtl number of the fluid and $Ra_H = \frac{g\beta}{\alpha_T \nu} H^3 \left| T_{neigh,\,i} - T_i \right|$, g is the gravity, β is the fluid coefficient of thermal volumetric expansion, α_T is the fluid thermal diffusivity, ν is the fluid kinematic viscosity, $T_{neigh,\,i}$ is the temperature in the neighbor VE or the exterior temperature, and H is the total solid swept height under analysis.

Equation (9) is valid for the entire Rayleigh number range – laminar, transition, and turbulent – with the fluid properties evaluated at the film temperature, that is, $T_{film} = (T_{neigh,i} + T_i)/2$, for all Prandtl numbers.[17]

b) forced convection[14,15]

$$h = \frac{k_f}{L}\left(0.064\ Pr^{1/3}\ Re_L^{1/2}\right)\text{, for } Re_L < 5 \times 10^5 \qquad (10)$$

or

$$h = \frac{k_f}{L}\left\{0.037\ Pr^{1/3}\ \left(Re_L^{4/5} - 23550\right)\right\},\ \text{for } Re_L > 5 \times 10^5 \qquad (11)$$

where $Re_L = \frac{v_f L}{\nu}$, v_f is the fluid velocity, and L is the total solid swept length under analysis.

3.1.2 Side face in contact with another element. It is assumed that there is no flow across a fluid–fluid boundary in the horizontal direction; flow is only in the vertical direction. While the assumption that there is a sudden temperature change from one block to the next does not appear to mimic reality, this assumption is considered acceptable in this simulation environment due to the large size of the VEs. In many cases, VEs are separated by bulkheads, and in the remaining cases, the flow from one element to the next is accounted for through the forced convection calculations in the vertical direction. This assumption greatly simplifies the defining equations and thus speeds the calculations.

If the interface is fluid–fluid or solid–solid, only conduction takes place between adjacent elements, due to the no-horizontal-flow assumption. The other possibility is a fluid–solid equipment interaction between the two elements, in which case heat transfer across the element face is ruled by convection.

For the fluid–fluid contact, since it is assumed that the fluid is not moving across the side faces, the heat transfer rate is given by

$$\dot{Q}_{l,\,i} = -\ U_{l,\,i} A_{l,\,i} (T_i - T_a),\ l = e, w, n, s \qquad (12)$$

where a indicates the adjacent element, and

$$U_{l,\,i} = \frac{k_f}{(l_{m,\,i} + l_{m,\,a})/2} \qquad (13)$$

where $l_{m,i}$ and $l_{m,a}$ are either the cell length or width, according to the index $m = x$ or y, if the ith or ath cell side face is east/west or north/south, respectively.

For the solid–solid contact, the heat transfer rate is also obtained from Equation (12), in which

$$U_{l,\,i} = \frac{1}{\frac{l_{m,\,i}/2}{k_i} + \frac{l_{m,\,a}/2}{k_a}} \qquad (14)$$

When the contact is of the type fluid–solid, convection takes place and Equation (12) is utilized. The appropriate heat transfer coefficient, h_l, is computed as in Equations (9)–(11), and

$$U_{l,\,i} = \frac{1}{\frac{1}{h_l} + \frac{l_{m,\,c}/2}{k_c}} \qquad (15)$$

where the index c indicates the solid element.

3.1.3 Top/bottom face in contact with another element. Since any element could have solid equipment or fluid inside, three types of interaction have to be taken into account, that is, (i) fluid–fluid, (ii) fluid–solid, and (iii) solid–solid.

(i) fluid–fluid
Both elements have fluid inside, and the heat flux is given by

$$\dot{Q}_{l,\,i} = \dot{m}_{l,\,i}\ c_{p,\,f}\ (T_a - T_i)\,, \qquad l = t, b \qquad (16)$$

where $\dot{m}_{l,\,i} = \rho_f\ v_i \frac{A_{l,\,i}}{2}$.
For natural convection, the estimated fluid velocity crossing the element face is $v_i = \alpha_T \left(\frac{g\beta}{\alpha_T \nu} |T_a - T_i| H\right)^{1/2}$, which is a natural convection representative scale.[14,15] It is also assumed that half of the element top/bottom face is crossed by the fluid in the upward direction, and half in the opposite direction.
In the case of forced convection, the estimated fluid velocity crossing the element face, v_i, is a known parameter from the air-conditioning system design.

(ii) fluid–solid
The heat transfer rate across the top/bottom element face follows from Equation (12), with $l = t$, b. $U_{l,i}$ is computed with Equation (15), and $l_{m,c}$ is replaced by $l_{z,c}$.

(iii) solid–solid
When both elements are solid pieces of equipment, the heat transfer rate also follows from Equation (12), with $l = t$, b. $U_{l,i}$ is given by Equation (15), and the lengths $l_{m,i}$ and $l_{m,a}$ are replaced by $l_{z,i}$ and $l_{z,a}$, respectively.

3.2 Heat transfer rates collected/rejected by cooling fluids (e.g. fresh and sea water) systems

In order to account for the different integrated system components and their cooling strategies, six VE types are defined based on their contents: (0) only air; (1) pure solid; (2) compact heat exchanger; (3) chilled fluid units; (4) internal fluid (closed-loop) cooled systems; and (5) external fluid (open-loop) cooled systems.

For element types 0 and 1, in Equation (1), $\dot{Q}_{conv,\,i} = 0$, since there are no cooling fluid (e.g. fresh or sea water) streams flowing across them. However, for element types 2 to 5, $\dot{Q}_{conv,\,i}$ is not zero and is a result of the adopted integrated system cooling strategy.

In the notional ship, each zone is cooled separately, with a combined air-conditioning, sea and fresh water cooling strategy. The system may contain cross-connects between zones to increase redundancy. For ease of discussion, the text refers to the internal fluid from this point on as 'fresh water', recognizing that it could be fresh, demineralized, or water–antifreeze mix. Similarly, it refers to the external fluid as 'sea water'.

The fresh water flows in a closed-loop collecting heat from the heat-generating systems within the zone, then rejecting heat to the cold external fluid (sea water) stream via a heat exchanger, or a chilled fluid unit or both, that is, there could be only the heat exchanger or the chilled fluid unit, or they could operate in series. For example, the use of a heat exchanger is not of interest when the available cold stream is at a higher temperature than the fresh water maximum temperature. Other cooling strategies may also be used, such as systems cooled by air conditioning and directly by sea water. The goal of this combined cooling strategy is that the zones and the entire integrated system temperature and relative humidity fields remain within acceptable and pre-established design limits.

The calculations start with the determination of the internal fluid temperature at the heat exchanger inlet in each integrated system zone. For that, a fresh water mixing section is accounted for before the heat exchanger inlet, in which the inputs are the mass flow rates that come from the output of each fresh water cooled component in the zone, and the output is the zone total fresh water mass flow rate. Therefore, a balance of energy in such mixing section allows for the calculation of the zone fresh water mixing section outlet temperature, which is the heat exchanger fresh water inlet temperature, as follows:

$$T_{fw,\,in} = \frac{\sum_{j=1}^{n_{eq}} \dot{m}_{fw,\,j} T_j}{\dot{m}_{fw}} \tag{17}$$

where $\dot{m}_{fw,\,j}$ is the fresh water mass flow rate coming out of component j; T_j is the temperature of component j (assumed equal to the fresh water coming out of it); $\dot{m}_{fw}$ is the total fresh water mass flow rate in the zone; and n_{eq} is the total number of fresh water cooled equipment in the zone. When $\dot{m}_{fw} = 0$ (pump off) in a particular zone, Equation (17) is not used.

The heat transfer rates collected/rejected by internal or external fluid (e.g. fresh or sea water), $\dot{Q}_{conv,\,i}$, are then calculated for each element type as follows.

(i) Element type 2 (heat exchanger)
The effectiveness-NTU method[14,18] is utilized to estimate the heat exchanger effectiveness, which could be applied to any type of compact heat exchanger.[18] Assuming a counterflow heat exchanger, the effectiveness is given by

$$\varepsilon_{hx} = \frac{1 - \exp\{-NTU(1 - C_{\min}/C_{\max})\}}{1 - (1 - C_{\min}/C_{\max})\exp\{-NTU(1 - C_{\min}/C_{\max})\}} \tag{18}$$

where $NTU = (UA)_{hx}/C_{\min}$; U and A are the global heat transfer coefficient and heat transfer area, respectively; subscript *hx* refers to the heat exchanger; $C_{\min} = (\dot{m}c)_i$ is the smallest heat capacity rate between the two streams (i = internal or external fluid) and $C_{\max}$ is the other one.
From the definition of effectiveness[14,18] and Equation (18), the heat exchanger sea water (e.g. sea water) outlet temperature is evaluated as follows:

$$T_{sw,\,out} = \frac{\varepsilon_{hx}\dot{m}_{fw}c_{fw}\left(T_{fw,\,in} - T_{sw,\,in}\right)}{\dot{m}_{sw}c_{sw}} + T_{sw,\,in} \tag{19}$$

where $\dot{m}$ and c are the mass flow rate and specific heat, respectively, T is the temperature, and subscripts *fw*, *sw*, *in* and *out* refer to fresh water, sea water, inlet and outlet, respectively. When $\dot{m}_{sw} = 0$ (pump off) in a particular zone, Equations (18) and (19) are not used; it is assumed that no flow occurs and thus $\dot{Q}_{conv} = 0$.
Therefore, the net heat transfer rate through the water streams crossing element type 2 is calculated as follows:

$$\dot{Q}_{conv,\,i} = \dot{m}_{fw}c_{fw}\left(T_{fw,\,in} - T_i\right) + \dot{m}_{sw}c_{sw}(T_{sw,\,in} - T_{sw,\,out}) \tag{20}$$

where subscript 'i' refers to the element type 2 under analysis, so that T_i is the element temperature, which is assumed to be equal to the fresh water outlet temperature as well, according to the thermodynamic assumption of uniform properties in a control volume.

(ii) Element type 3 (chilled fluid unit):
The net heat transfer rate through the fresh water stream crossing element type 3 is calculated as follows:

$$\dot{Q}_{conv,\,i} = \dot{m}_{fw} c_{fw} \left(T_{fw,\,out} - T_i \right) \tag{21}$$

where subscript '*i*' refers to the element type 3 under analysis, and $T_{fw,\,out}$ is the fresh water heat exchanger outlet temperature.
In element type 3, $\dot{Q}_{gen} \leq 0$, which is a design parameter corresponding to the nominal refrigeration rate of the selected chilled fluid unit, in which the equal sign accounts for the situation when the unit is turned off. In this unit, it is assumed that heat is rejected to a sea water stream that extracts heat from the condenser.

(iii) Element type 4 (fresh water cooled components):
The net heat transfer rate through the fresh water stream crossing any element type 4 in the zone is calculated as follows:

$$\dot{Q}_{conv,\,i} = \dot{m}_{fw} c_{fw} (T_{cw,\,out} - T_i) \tag{22}$$

where subscript '*i*' refers to the element type 4 under analysis, and $T_{cw,\,out}$ is the chilled fluid unit fresh water outlet temperature.

Some components could have dedicated cooling systems, which could be a refrigeration system or a secondary heat exchanger. In the case of a dedicated refrigeration system, heat is extracted from the load through the evaporator, but the heat transfer rate that is rejected by the condenser inside the element is given by

$$\dot{Q}_{gen} = \frac{1+\eta}{\eta} \dot{Q}_{evap,\,DCS} \tag{23}$$

where $\dot{Q}_{evap,\,DCS}$ is a design parameter corresponding to the nominal refrigeration rate of the refrigeration unit that was selected to cool the load locally, which is meant to match the component heat generation rate, and η is the nominal unit thermal efficiency (or COP – coefficient of performance).

In the case of a secondary heat exchanger, $\dot{Q}_{gen}$ is assumed to be the component heat generation rate.

(iv) Element type 5 (auxiliary sea water cooled systems)

The net heat transfer rate through the auxiliary water stream crossing any element type 5 in the zone is calculated as follows:

$$\dot{Q}_{conv,\,i} = \dot{m}_{asw} c_{sw} (T_{sw,\,in} - T_i) \tag{24}$$

where subscript '*i*' refers to the element type 5 under analysis.

4. Numerical method

Equation (1) defines a system of N ordinary differential equations with time as the independent variable, along with the initial conditions, for the unknowns T_i, that is, the temperatures of each VE. Once the temperatures of each VE are known, the corresponding relative humidity follows immediately from Equations (2) and (3).

The unsteady system of equations is integrated in time, from given initial conditions, explicitly using a fourth-order Runge–Kutta method.[19] If the transient solution is of no interest, the system is solved directly for the steady-state solution. The time derivative terms in the ordinary differential equations' system defined by Equation (1) are dropped and a system of N non-linear algebraic equations is obtained. In this case the unknowns are the steady-state temperatures at the center of each elemental volume. The resulting non-linear system of algebraic equations is solved using a Newton–Raphson method. The system of equations is linearized with respect to the cell center temperatures, after which the VEs' relative humidities are computed based on Equations (2) and (3).

The convergence of the numerical results was verified by successive mesh refinements[20] and monitoring the variation of the Euclidean norm of the temperatures numerical solution in the entire domain. The results of a less refined mesh (mesh 1) are compared to the results of a more refined mesh (mesh 2), and the refinements stop when the mesh refinement relative error, ε_{mesh}, criterion is satisfied, then mesh 1 is selected as the converged mesh, as follows:

$$\varepsilon_{mesh} = \frac{\left| \|T\|_{mesh1} - \|T\|_{mesh2} \right|}{\|T\|_{mesh1}} \leq 0.01 \tag{25}$$

Both the mesh and the numerical results were processed for graphical visualization in different planes and surfaces. For that, a free graphic software produced by the Lawrence Livermore National Laboratory was utilized.[7]

5. Results and discussion

As an example of a complex and integrated system analysis using the mathematical model developed in Section 2, 3D simulations are performed in order to determine the temperature and relative humidity distributions inside an all-electric ship for a baseline MVDC architecture, under different operating conditions. Figure 2 summarizes the distribution of the components of the notional all-electric ship baseline MVDC architecture, their respective zones, and a proposal for the general cooling strategy, including sea water, fresh water, and air-conditioning cooling

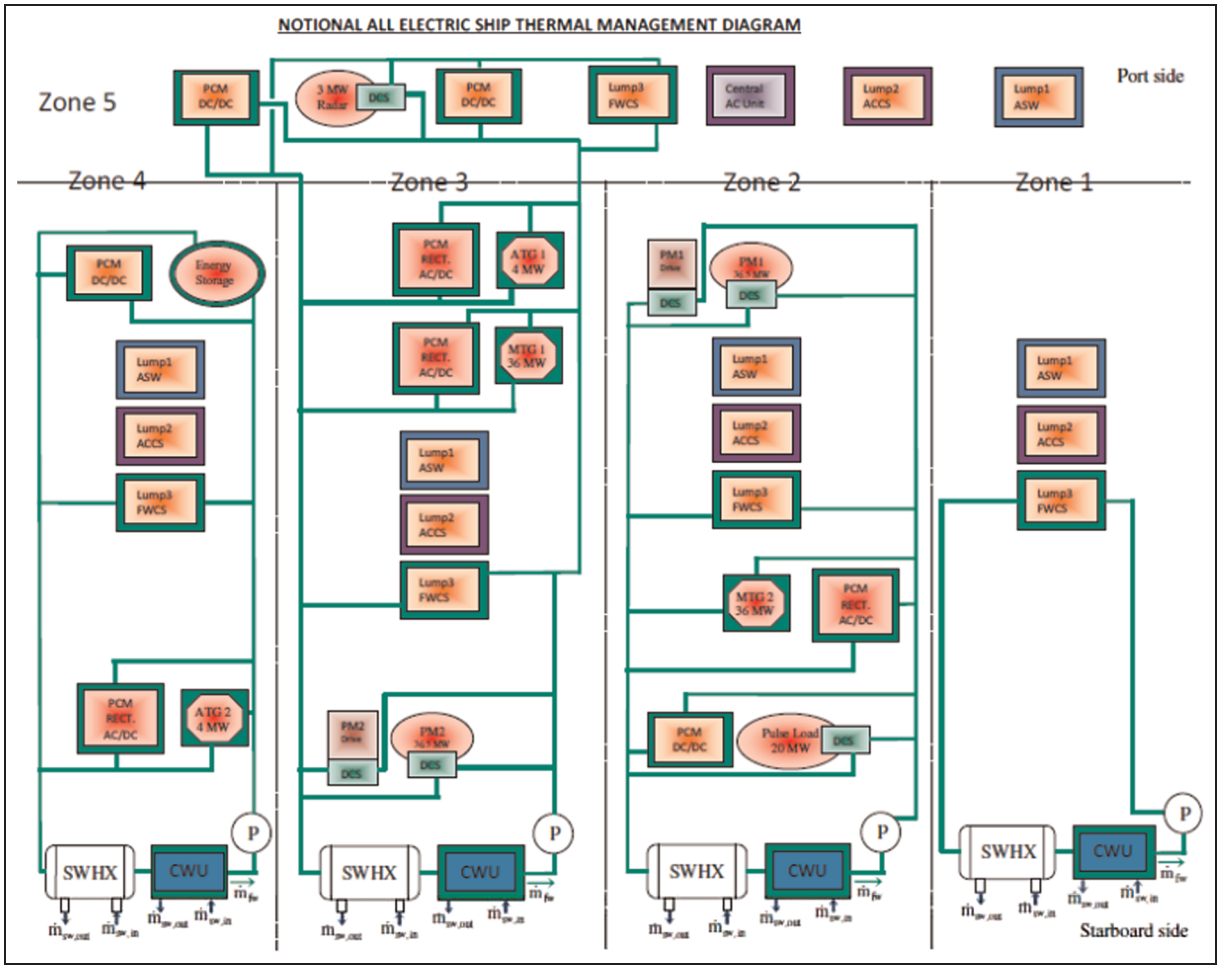

Figure 2. Schematic diagram of notional equipment and cooling circuits, where AC – air conditioning; ACCS – air conditioned cooled system; AC/DC – alternating to direct current; ASW – auxiliary sea water cooled; ATG – auxiliary gas turbine; CWU – chilled water unit; DCS – dedicated cooling system; FWCS – fresh water cooled system; $\dot{m}$– mass flow rate; MTG – main gas turbine generator; P – pump; PCM – power conversion module; PM – propulsion motor; RECT – rectifier, and SWHX – sea water heat exchanger.

systems. The larger loads are shown individually (e.g. gas turbines, pulse load), whereas the smaller loads have been lumped together for simplicity in auxiliary sea water, fresh water, and air-conditioning cooled loads.

In the steady-state cases studied in this paper, the iterative process required 5–10 min to achieve convergence, that is, the Euclidean norm of the residual of the system was less than 10^{-3}. Hence, a low computational time to obtain the steady-state solution was required in all cases. The computer used to perform the simulations was a laptop with a Pentium (R) Dual-Core central processing unit (CPU) T4300 @ 2.10 GHz, 3 GB RAM, 64-bit operating system.

All simulations were performed in a LINUX operating system. A C++ code was written to generate the 3D mesh to represent the ship as a computational domain. Numerical results were produced with a Fortran code based on the mathematical model described in Section 2. The input data for the computational simulation of the systems response were selected according to the geometry, components, operating, and environmental conditions of the case studies simulated in this paper.

The ship is divided into small compartments (VEs) and equipment is placed in one or more grid elements according to their actual dimensions. The procedure was designed to start from the equipment bounding box desired location for the vertex with the lowest x-, y-, and z-coordinates, to which equipment length (x-direction), width (y-direction), and height (z-direction) are added to determine the other seven vertices. The eight resulting equipment bounding box vertices coordinates are then compared with the nodal coordinates of all grid elements in order to determine the mesh VEs to which the equipment should be allocated.

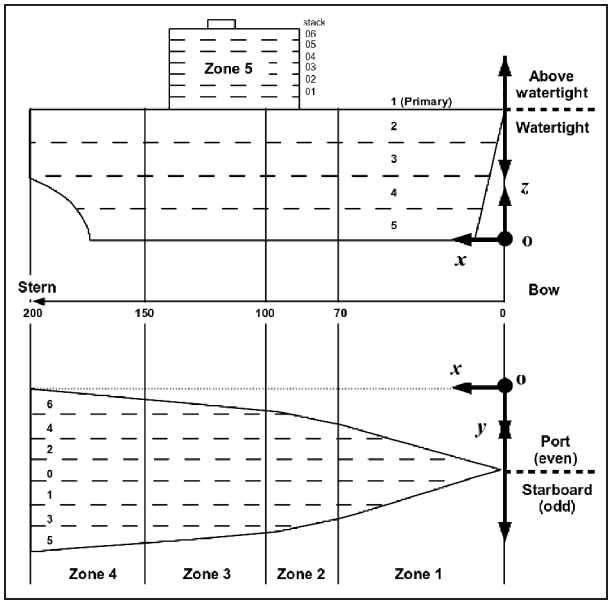

Figure 3. Ship zones distribution.

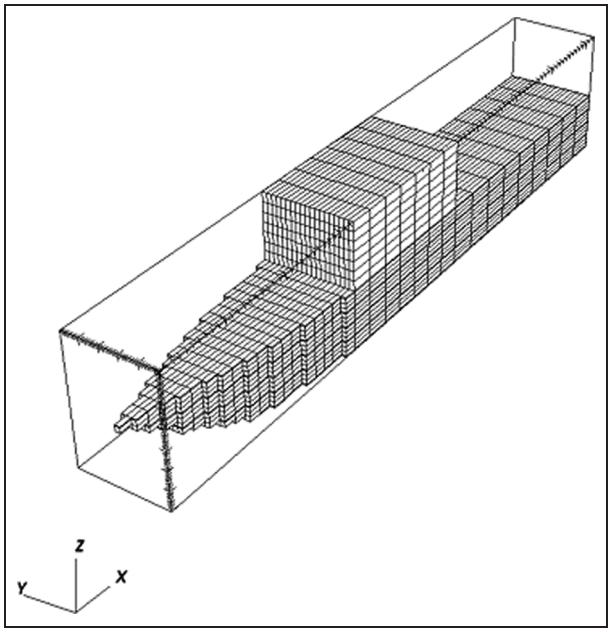

Figure 4. Notional all-electric ship converged mesh.

Table 1. Notional all-electric ship dimensions.

Direction	Length (m)	Divisions
Bow to stern (length)	184	200
Port to starboard (beam)	24	7
Baseline to watertight deck (depth)	16	4
Watertight deck to top of superstructure	18	7

In the present work, in order to assess conceptually the possibility of obtaining the ship's internal temperature distribution with the proposed model and computational application, a notional all-electric ship baseline MVDC architecture was utilized. In addition, all small and medium thermal loads were lumped in their respective zones with an estimated total value. Besides the small and medium loads, all ship big thermal loads shown in Figure 2 were accounted for in the simulations.

The ship discretization follows the notional data standards[21] shown in Figure 3. The ship geometry has 11 deck divisions (4 below and 7 above watertight), 200 divisions in the bow to stern direction, and 7 divisions in the port to starboard direction.

The resulting 3D geometry is shown Figure 4. The converged grid according to the criterion of Equation (25) had a total of 9410 elements. Grid generation was constructed with the notional ship physical dimensions.[21] The notional all-electric ship geometric dimensions are shown in Table 1.

The external conditions considered in the two simulations performed in this work are:

1. average local sun irradiation: 400 W m^{-2} (top, east, and north walls) and 0 W m^{-2} (west and south walls);
2. frontal wind speed: 10 m/s;
3. frontal sea water speed: 10 m/s;
4. two different atmospheric air temperatures: 260 and 305 K; and
5. two different sea water temperatures: 280 and 288 K, which correspond to 260 and 305 K (10 and 90°F) air temperature days, respectively.

The mesh was non-uniform, that is, the cells had variable sizes to allow for the representation of the ship in the domain, and to place the heat generation sources appropriately in each ship zone. The notional all-electric ship equipment list per zone and respective heat generation rates are shown in Table 2.

Regarding the thermal design, sea water heat exchangers (SWHXs) with known global heat transfer coefficients, U [W m^{-2} K^{-1}], and areas, A [m^2], were allocated to zones 1, 2, 3 and 5, and 4, such that (U, A) = (100, 100); (100, 1000); (100, 2000), and (100, 100), respectively. Also chilled water units (CWUs) were allocated to zones 1, 2, 3–5, and 4, with known refrigeration capacity rates of 100, 500, 500, and 100 kW, respectively. Equal fresh and sea water total mass flow rates of 8, 60, 60, and 10 kg s^{-1} were selected to zones 1, 2, 3–5, and 4, respectively. For the fresh water circuit, the total zone fresh water mass flow rate was divided among the components cooled by fresh water within the zone according to the last column of Table 2. The mass flow rate fractions add up to one in all zones, except in zones 3 and 5, which are cooled jointly by

Table 2. Notional all-electric ship equipment list, in which DC/DC - direct to direct current; AC/DC - alternating to direct current; ES - energy storage; STBD - starboard; FEL - free-electron laser, and the definitions of all other abbreviations are given in the label of Figure 2.

Electrical equipment	Power (kW)	Efficiency	Heat generation rate (kW)	Fresh water mass flow rate fraction
				Zone 5
RADAR PCM DC/DC	3866	0.97	115.98	0.040
RADAR	3750	0.85	562.5	0.100
Lump1 (ASW)			30	
Lump2 (ACCS)			10	
Lump3 (FWCS)			30	0.010
TOTAL			**748.48**	**0.150**
				Zone 4
ATG2	4000	0.96	160	0.175
PCM AC/DC	3840	0.96	153.6	0.175
ES PCM DC/DC	4000	0.97	120	0.150
Lump1 (ASW)			100	
Lump2 (ACCS)			200	
Lump3 (FWCS)	2965	0.85	444.75	0.500
TOTAL			**1178.35**	**1.000**
				Zone 3
MTG1	36,000	0.98	720	0.155
PCM AC/DC	35,280	0.98	705.6	0.155
ATG1	4000	0.96	160	0.050
PCM AC/DC	3840	0.96	153.6	0.050
PORT Motor Drive	37,200	0.98	744	0.170
PORT Motor	36,500	0.98	730	0.170
Lump1 (ASW)			200	
Lump2 (ACCS)			200	
Lump3 (FWCS)	3890	0.85	583.5	0.100
TOTAL			**4196.7**	**0.850**
				Zone 2
MTG2	36,000	0.98	720	0.200
PCM AC/DC	35,280	0.98	705.6	0.200
STBD Motor Drive	37,200	0.98	744	0.250
STBD Motor	36,500	0.98	730	0.200
Pulsed Load (FEL)	25,000	0.12	36.67	0.050
Lump1 (ASW)			100	
Lump2 (ACCS)			200	
Lump3 (FWCS)	3241	0.85	486.15	0.100
TOTAL			**3722.4**	**1.000**
				Zone 1
Lump1 (ASW)			36.27	
Lump2 (ACCS)			50	
Lump3 (FWCS)	2790	0.85	418.5	1.000
TOTAL			**504.77**	**1.000**

one SWHX and CWU, so that their fresh water mass flow rate fractions together add up to one.

Figure 5 shows the spatial distribution of all pieces of equipment listed in Table 2 inside the ship. Arbitrary locations and dimensions were selected to conduct the simulations presented in this work. However, the equipment locations and dimensions can be easily changed in the input data according to any mechanical notional ship design.

In both scenarios analyzed in this work, it was assumed that the ship's draft was 10 m, and the assumed known initial relative humidity was $\varphi_{i0} = 0.8$ (80%). Only steady-state simulations were performed in this study. However, as

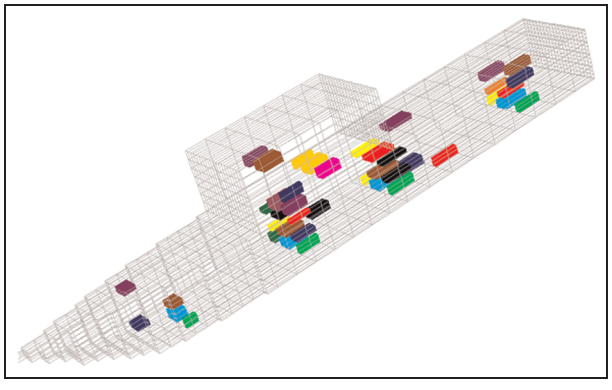

Figure 5. Components distribution inside the ship.

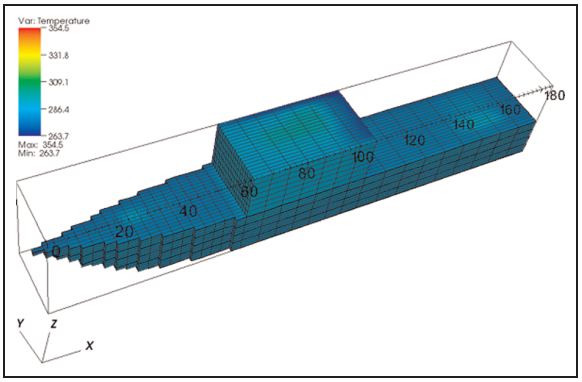

Figure 6. Ship external temperature field on a 260 K (10°F) day.

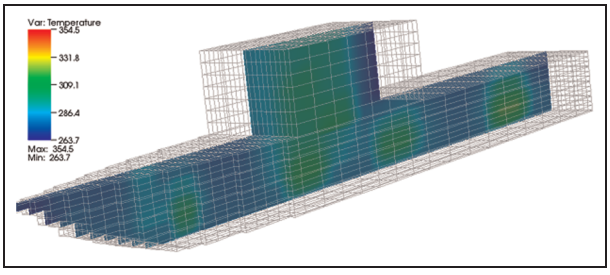

Figure 7. Ship midplane temperature field on a 260 K (10°F) day.

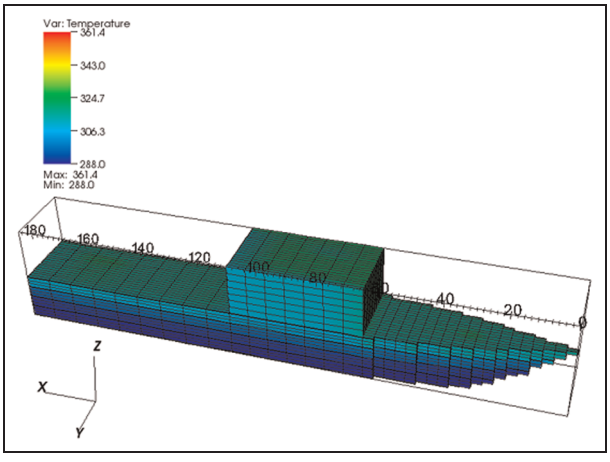

Figure 8. Ship external temperature field on a 305 K (90°F) day.

presented previously in the text, the developed mathematical model allows for integrated system transient simulations.

The resulting external temperature field for the first simulation in a 260 K (10°F) day is shown in Figure 6. The maximum observed temperature within the ship was 354.5 K, as is shown in the legend of Figure 6, which demonstrates the effectiveness of the fresh and sea water cooling

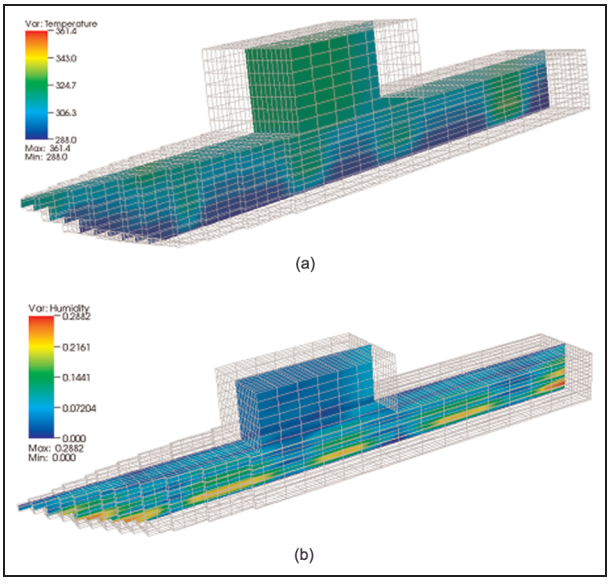

Figure 9. Ship midplane temperature (a) and relative humidity (b) field on a 305 K (90°F) day.

strategies to extract the large heat generation rates shown in Table 2 out of the ship, and keep the cooling water temperature below boiling point throughout the ship.

The results are further analyzed internally in the ship midplane in Figure 7. As expected, the highest temperatures occur in zones 2 and 3, where heat generation is higher.

The resulting external temperature field for the second simulation in a 305 K (90°F) day is shown in Figure 8. The maximum temperature within the ship was 361.4 K, as is shown in the legend of Figure 8, which again demonstrates the effectiveness of the water cooling strategies to extract heat out of the ship, even on a hotter day than the previous simulation. In this simulation, it is possible to notice the water line on the hull through the surface temperature distribution.

Next, the results are analyzed internally in the ship midplane, shown in Figure 9(a). Again, the highest temperatures occur in zones 2 and 3, where heat generation is higher. Figure 9(b) illustrates the resulting humidity field in the ship's midplane. It is interesting to note that as temperature increases, the relative humidity decreases in air VEs, as expected thermodynamically. In addition, in solid VEs, the model sets $\varphi_i = 0$, therefore it is possible to identify where solid equipment is located based on the resulting relative humidity distribution.

Figure 10 summarizes the fresh water temperature results within all ship zones. In Figure 10(a), the results for a 260 K (10°F) day are shown, and for a 305 K (90°F) day in Figure 10(b). The results show that the design-established condition of not reaching the water boiling point was achieved, by checking the maximum calculated fresh water temperature within the zones. In addition,

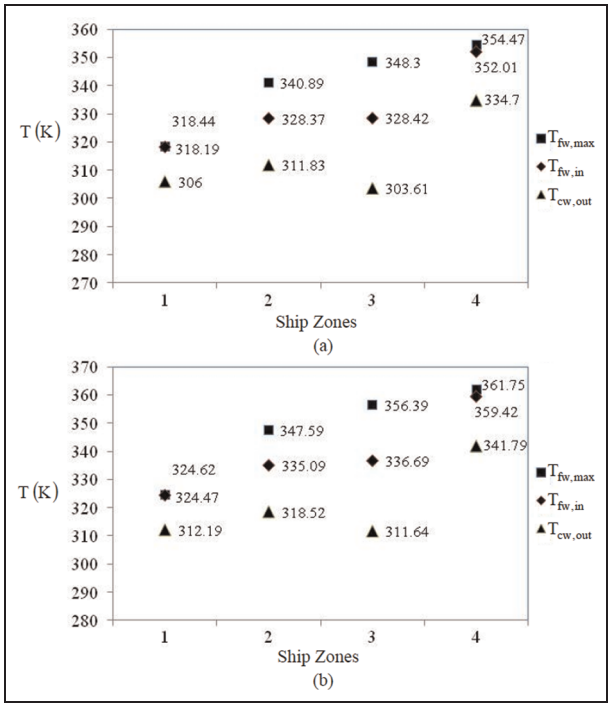

Figure 10. Fresh water temperatures within all zones (maximum, heat exchanger inlet, and chilled water unit outlet) for (a) a 260 K (10°F) day and (b) a 305 K (90°F) day.

results show that for zones 1 and 4, the maximum temperature approximately matches the heat exchanger inlet temperature calculated with Equation (17), but this is not the case for zones 2 and 3–5. In zone 1, the total fresh water mass flow rate was directed exclusively to Lump3 (fresh water cooled system – FWCS), since it is the only heat-generating component cooled by fresh water, according to Table 2, but in the other zones, the zone total fresh water mass flow rate was divided among the zone components, as shown in Table 2. The analysis of Figure 10 presents the opportunity to find an optimal fresh water mass flow rate division within the zones so that the gap between maximum component output and SWHX inlet temperatures is narrowed to a minimum value, so that the utilization of cooling resources is maximized, therefore maximizing the cooling system performance. In other words, the zone total fresh water mass flow rate is optimally distributed among the zone fresh water cooled components, so that minimal fresh water output temperature is achieved in the zone components. The results for zone 4 in Figure 10 are one example of such optimal division.

Finally, one of the main objectives of this work was to develop a computational tool that required low computational time to provide solutions for each tested configuration in order to allow for an effective design and optimization procedure. The largest computational time required for obtaining the results for the cases presented in this work was 560 s, that is, less than 10 min, using as initial value a temperature field in equilibrium with the external environment, which is the expected worst scenario. Whenever solutions are available from previous simulations, the use of restart files dramatically reduces the required computational time for convergence to the new case solution. Based on these observations, it is reasonable to state that such objective has also been accomplished.

6. Conclusions

In this paper, a general transient computational model for the thermal management of physical systems with heat sinks and sources, fresh and sea water (or any other cooling fluid), as well as air-conditioning cooling strategies, has been developed. The model was tested with steady-state simulations of a notional all-electric ship. The obtained results illustrate how the VEM could be used to calculate the temperature and relative humidity fields anywhere in the domain, for any number of VEs adopted in the simulations. The model allows for the use of a relatively coarse mesh to discretize the domain and still obtain converged numerical results, with low computational time, in spite of the diverse nature of the components inside the domain. Therefore, it is expected that, after experimental validation and model adjustment to ensure the accuracy of results, the developed application could be used as an efficient tool for complex and integrated systems thermal design, control and optimization.

Funding

This work was supported by the ONR (grant – N00014-08-1-0080).

References

1. Liu P, Georgiadis MC and Pistikopoulos EN. Advances in energy systems engineering. *Ind Eng Chem Res* 2011; 50: 4915–4926.
2. Jogwar SS, Baldea M and Daoutidis P. Tight energy integration: dynamic impact and control advantages. *Comput Chem Eng* 2010; 34: 1457–1466.
3. Mustafiz S and Islam MR. State-of-the-art petroleum reservoir simulation. *Pet Sci Technol* 2008; 26: 1303–1329.
4. Vargas JVC, Stanescu G, Florea R, et al. A numerical model to predict the thermal and psychrometric response of electronic packages. *ASME J Electron Packag* 2001; 123: 200–210.
5. Ordonez JC, Vargas JVC and Hovsapian R. Modeling and simulation of the thermal and psychrometric transient response of all-electric ships, internal compartments and cabinets. *Simulation* 2008; 84: 427–439.
6. Dias FG, Souza JA, Ordonez JC, et al. Notional all-electric ship thermal simulation and visualization. In: *proceedings of the 2009 IEEE electric ship technologies symposium*, Baltimore, MD, ESTS Proceedings, New York: IEEE, 2009.

7. VisIt 1.11.1 Manual. Livermore, CA: Lawrence Livermore National Laboratory, 2008.
8. Souza JA, O'Lary FM, Hovsapian R, et al. Visualization tool for notional all-electric ships data bases. In: *proceedings of the 2010 grand challenges in modeling and simulation*, Ottawa, Canada, GCMS Proceedings, 11–14 July 2010.
9. Wagner B. All-electric ship could begin to take shape by 2012. *NDIA's Business and Technologies Magazine*, November 2007.
10. Smith AN, Ellis RL, Bernardes JS, et al. Thermal management and resistive rail heating of a large-scale naval electromagnetic launcher. *IEEE Trans Magn* 2005; 41: 235–240.
11. Kanerva S and Hansen JF. State of the art in electric propulsion - viewpoint on redundancy. In: *IEEE electric ship technologies symposium*, Baltimore, MD, 2009, pp.499-504.
12. Soman RR, Davidson EM and McArthur SDJ. Using functional failure mode and effects analysis to design the monitoring and diagnostics architecture for the zonal MVDC shipboard power system. In: *IEEE electric ship technologies symposium*, Baltimore, MD, 2009, pp.123–128.
13. Fletcher CAJ. *Computational techniques for fluid dynamics*. Vol. 1. Berlin: Springer, 1991.
14. Bejan A. *Heat transfer*. New York: Wiley, 1993.
15. Bejan A. *Convection heat transfer*. 2nd ed. New York: Wiley, 1995.
16. Duffie JA and Beckman AA. *Solar energy thermal processes*. New York: Wiley, 1974, pp.34–37.
17. Churchill SW and Chu HHS. Correlating equations for laminar and turbulent free convection from a vertical plate. *Int J Heat Mass Transfer* 1975; 18: 1323–1329.
18. Kays WM and London AL. *Compact heat exchangers*. 3rd ed. New York: McGraw-Hill, 1984.
19. Kincaid D and Cheney W. *Numerical analysis*. Belmont, CA: Wadsworth, 1991.
20. Editorial. Journal of heat transfer editorial policy statement on numerical accuracy. *ASME J Heat Transfer* 1994; 116: 797–798.
21. Amy J. Load analysis 2007 for ESRDC3 REV2.xls. *Electric Ship Research and Development Consortium*, 2008.

Author biographies

José VC Vargas is a Visiting Professor at the Department of Mechanical Engineering and the Center for Advanced Power Systems at Florida State University, and Associate Professor at the Department of Mechanical Engineering at the Federal University of Paraná, Curitiba, Brazil. His research interests include biofuels, alternative energy, constructal theory, and modeling, simulation, and optimization of complex integrated systems.

Jeferson A Souza is an Adjoint Professor at the Federal University of Rio Grande, Brazil, and formerly Research Associate at the Center for Advanced Power Systems and Department of Mechanical Engineering at Florida State University. His research interests include thermal engineering, transport phenomena, alternative energy, and advanced computer programming.

Rob Hovsapian is a Research Scientist at the Department of Energy Idaho National Laboratory, INL, and formerly Program Manager of the Electric Ship Research and Development Consortium (ESRDC) at the Center for Advanced Power Systems at Florida State University. His research interests include thermal engineering and alternative energy.

Juan C Ordóñez is Associate Professor at the Department of Mechanical Engineering and the Center for Advanced Power Systems at Florida State University. His research interests include thermodynamic optimization, constructal theory, and thermal modeling and management of advanced energy systems.

Tim Chiocchio is an Assistant in Research at the Center for Advanced Power Systems at Florida State University. His research interests include real-time and offline modeling and simulation of power systems, especially focused on superconducting fault current limiters, electric machines and power electronic converters.

Dr Julie Chalfant is a research scientist in the MIT Sea Grant College Program and a member of the ESRDC. Her background also includes experience in ship operation and repair as an officer in the United States Navy.

Prof. Chryssostomos Chryssostomidis is Doherty Professor of Ocean Science and Engineering, Director of the MIT Sea Grant College Program and a faculty member of the Department of Mechanical Engineering of MIT. His research interests include autonomous underwater vehicles and advanced ship design of the all-electric ship.

Emerson Dilay is a Research Associate at the Center for Advanced Power Systems and Department of Mechanical Engineering at Florida State University. His research interests include thermal engineering, alternative energy, and advanced computer programming.